Contents lists available at ScienceDirect

Journal of Molecular Catalysis. A, Chemical

journal homepage: www.elsevier.com

Journal Cover Image

In-situ ATR-IR study of surface reaction during aqueous phase reforming of glycerol, sorbitol and glucose over Pt/γ-Al_2O_3

Jungseob So [a, b], Yoona Chung [a], David S. Sholl [a], Carsten Sievers [a, b, *]

[a] School of Chemical & Biomolecular Engineering, Georgia Institute of Technology, Atlanta, GA, 30332, USA
[b] Renewable Bioproducts Institute, Georgia Institute of Technology, Atlanta, GA, 30332, USA

ARTICLE INFO

Keywords:
Biomass
Water-gas shift
Carbon monoxide
Polyol
Sugar

ABSTRACT

Surface reactions involved in aqueous phase reforming of glycerol, sorbitol and glucose over Pt/γ-Al_2O_3 are studied by in-situ attenuated total reflection infrared (ATR-IR) spectroscopy. In these experiments aqueous solutions of the reactants are flowed over a catalyst layer that is coated on the internal reflection element of the spectroscopic cell. Linearly bound CO (CO_L) and bridging CO (CO_B) are readily formed on the Pt particles at 24–72 °C. The relative abundance of CO in different environments and the rates of formation and conversion of these species provide insight into the reaction path of different oxygenates. Even at 24 °C, CO_B can be converted by the water-gas shift reaction. During the conversion of sorbitol and glucose, the formation and conversion of adsorbed CO is affected by the presence of co-adsorbed reactants or by-products. In addition to CO, surface bound alkoxy species are observed during the conversion of sorbitol and glucose.

1. Introduction

In the 20th century, the petrochemical industry developed numerous processes for converting hydrocarbons into commodities. However, diminishing reserves of fossil feedstocks and related carbon dioxide emissions have motivated an intensive search for renewable sources of fuels and chemicals. Biomass is considered as a sustainable long-term solution as feedstock for many products [1–3]. Aqueous Phase Reforming (APR) of biomass has gained significant attention as a promising heterogeneously-catalyzed process for converting oxygenated carbohydrates, such as sugars (e.g., glucose) and polyols (e.g., methanol, ethylene glycerol, glycerol and sorbitol), into H_2 and CO_2 at temperatures around 230 °C (Scheme 1) [4–7]. Thus, this process can provide the hydrogen needed in many other biorefining operations, such as hydrodeoxygenation [1].

APR has several advantages over the conventional steam reforming processes. Specifically, APR operates at relatively low temperatures and somewhat higher pressures compared to industrial steam reforming processes. This eliminates the need to evaporate both water and the oxygenated hydrocarbons, leading to energy saving [7,8]. In addition, a hydrogen stream with low amounts of CO is produced in a single reactor because APR is performed at temperatures where the water-gas shift (WGS) equilibrium is favorable for the forward reaction [4,7]. Moreover, APR is conducted at pressures (typically 15–50 bar) where pressure-swing adsorption and membrane technologies can efficiently separate hydrogen from the effluent [8]. In principle, APR can convert any polyol, but the H_2 yield decreases notably with larger molecules, such as sorbitol [9]. Even lower yields were reported for the conversion of glucose [9]. The reaction pathways of APR of biomass-derived polyols have been studied by many research groups, but the reasons for the strong dependence of the H_2 yield on the feedstock are not entirely understood [9–12].

Effective catalysts for APR require high activity for C—C bond cleavage and the WGS reaction, but activity for CO hydrogenation can reduce the hydrogen selectivity and result in the formation of light alkanes (i.e., methane and ethane) [13]. When acidic supports catalyze dehydration steps, various reaction products, such as alcohols, aldehydes, and alkanes, can be co-produced [11]. In particular, the formation of alkanes by repeated dehydration and hydrogenation steps was reported [14]. Among a set of monometallic catalysts (i.e., Pt, Ni, Ru, Rh, Pd, Ir), Pt was found to have the best combination of activity for C—C bond cleavage and the WGS reaction [6]. Among the different supports (i.e., TiO_2, Al_2O_3, carbon, SiO_2, ZrO_2, CeO_2, and ZnO) investigated for

Abbreviations: ν, stretching mode; δ, deformation mode; APR, means aqueous phase reforming; ATR-IR, attenuated total reflection infrared (spectroscopy); WGS, water-gas shift; CO_L, CO linearly bound to Pt; CO_B, CO bridging CO on Pt; H*, dissociatively adsorbed hydrogen on Pt.

* Corresponding author at: School of Chemical & Biomolecular Engineering, Georgia Institute of Technology, Atlanta, GA, 30332, USA.
Email address: carsten.sievers@chbe.gatech.edu (C. Sievers)

https://doi.org/10.1016/j.mcat.2019.110423
Received 15 April 2019; Received in revised form 21 May 2019; Accepted 22 May 2019
Available online xxx
2468-8231/

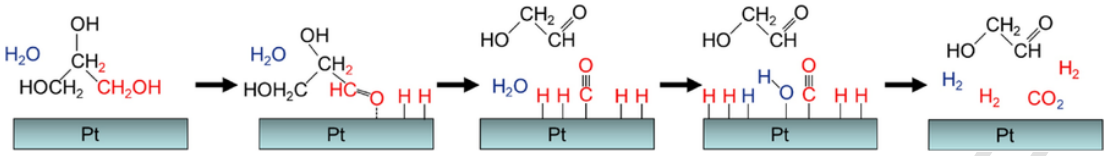

Scheme 1. Reactions involved in APR of glycerol.

Pt particles, Al_2O_3 exhibited the highest hydrogen selectivity (>90%) [15]. A large particle size of Pt is beneficial for H_2 selectivity since low index Pt surfaces favor C—C bond cleavage [16]. However, several studies showed that CO oxidation by WGS reaction is the rate-limiting step in APR, and the reaction is strongly inhibited by adsorbed hydrogen and CO on the surface [4,5,17].

CO oxidation on metal surfaces is a traditional reaction of interest in surface science [18–20], and many efforts have already been made to understand this reaction at the molecular level, often studying CO conversion experimentally or theoretically on single crystal surfaces in ultra-high vacuum [21–24]. Small amounts of H_2O in the gas phase can convert CO to CO_2 via the WGS reaction even at low temperatures [21,25]. In addition, DFT calculations showed that the activation barrier of CO oxidation is reduced in the presence of H_2O vapor [25,26]. These studies cannot be directly applied to the APR reaction conditions since the chemical potential of water is much higher, and water can affect reaction paths by solvating surface species and transition states [27]. Moreover, it is important to account for the presence of a variety of exposed facets in supported metal catalysts.

Attenuated total reflectance infrared (ATR-IR) spectroscopy is a powerful approach to probe reactions on solid-liquid or solid-gas interfaces. A study of methanol reforming over Pt/Al_2O_3 in vapor and liquid phase showed that CO is formed as intermediate on Pt and that the surface coverage by CO decreases as the partial pressure of H_2O increases [17]. In the same study, it was shown that product inhibition by adsorbed hydrogen reduces the number of surface sites that are available for activating methanol. H_2O also has a positive effect on the rate of CO oxidation over Pd/Al_2O_3 and causes a red-shift of the stretching vibration of CO species compared to dry conditions [28]. Similarly, a large red-shift of the stretching vibration of CO adsorbed on Pt/Al_2O_3 indicated that the C–O bond is weakened by formation of an activated CO-water complex [29]. These studies provide insight into the nature of surface species on metal particles during APR and related reactions. However, few studies directly investigate the rates of formation and conversion of surface bound CO. Recently, our group reported that Pt/Al_2O_3 readily converts glycerol to adsorbed CO at room temperature once metal sites are cleaned by exposing them to hydrogen and oxygen saturated water in an alternating order and that bridging CO can be converted by water gas shift even at room temperature [30].

In addition to the formation of CO and its oxidation by the WGS reaction, it is important to understand how APR is affected by the presence of additional surface species that can be formed from biomass-derived oxygenates containing multiple functional groups. Various surface intermediates (e.g., acetate, carbonate, crotonaldehyde, acetyl, acetone, and adsorbed linearly bound and bridging CO) were identified in spectroscopic studies of ethanol conversion over supported metal catalysts, such as Pt/Al_2O_3 and Rh/Al_2O_3 [31–35]. The key difference between surface intermediates on single crystal metal surfaces and metal-oxide-supported metal particles is the possible presence of oxygenated surface species on the support and at the metal-support interface. Moreover, the presence of multiple functional groups in the same molecule creates different possibilities of forming bonds to the surface, which may be mutually exclusive [27]. For example, glycerol adsorbs strongly on Lewis acidic metal oxides by forming a cyclic species, which involves a bridging alkoxy bond between a primary alcohol group and the Lewis acid site as well as a non-dissociative interaction of the other primary alcohol group with the same site [36,37]. Under conditions similar to the operating conditions of APR (i.e., 190–225 °C), ketones or aldehydes can also form on the surface of Pt/Al_2O_3 [11], and ketones can strongly adsorb on supported metal particles under similar conditions [38].

Here, we report the effect of size and functionality of oxygenate molecules on the formation of surface species on 5 wt% $Pt/\gamma\text{-}Al_2O_3$ in aqueous phase using in-situ ATR-IR spectroscopy. Specifically, kinetics of formation and conversion of linearly bound and bridging CO from glycerol, sorbitol, and glucose are studied at different temperatures, and the effect of co-adsorbed surface species is discussed.

2. Experimental

2.1. Materials

Glycerol, sorbitol, and glucose (99%) and 5 wt% Pt on $\gamma\text{-}Al_2O_3$ were used as received from Sigma Aldrich. A Barnstead NANO unit was used to further purify deionized water up to 18.2 MΩ/cm. All H_2, O_2, and He gases were purchased from Airgas with ultra-high purity grade (UHP, grade 5).

2.2. Catalyst characterization

X-ray diffraction (XRD) patterns of 5 wt% Pt on $\gamma\text{-}Al_2O_3$ were obtained with a Philips X'pert diffractometer using an X'celerator module using Cu Kα radiation. Diffractograms were collected at incident angles from $2\theta = 5^\circ$ to 70° with a step size of 0.0167°. Nitrogen physisorption measurements were taken using a Micromeritics ASAP 2020 Physisorption Analyzer. Samples were degassed under vacuum at 250 °C for 4 h prior to analysis. The surface area of the sample was calculated from the adsorption isotherm in the region $0.05 < P/P_0 < 0.3$, based on the BET method [39]. The BJH method [40] was also adopted to calculate average pore diameters of the sample in the region $0.05 < P/P_0 < 0.99$. Pyridine adsorption followed by IR spectroscopy was performed using a Thermo-Nicolet 8700 FT-IR spectrometer with a MCT/A detector. For every spectrum, 64 scans were accumulated at a resolution of 4 cm^{-1}. The sample was pressed into self-supported wafer and then mounted into a custom-built vacuum chamber with ZnSe windows. The activation of the catalyst wafer was conducted at 500 °C at $<10^{-6}$ mbar for 12 h, and a background spectrum was taken after lowering the temperature to 150 °C. Pyridine was introduced into the chamber at a partial pressure of 0.1 mbar for 30 min. The spectrum of adsorbed pyridine was taken after the chamber was evacuated for 30 min. After the experiment, the density of the catalyst wafer was determined by weighing a cutout of the wafer with a diameter of 6.35 mm (1/4 inch). The concentrations of Lewis and Brønsted acid sites were determined based on the integrated areas of the peaks of chemisorbed pyridine and pyridinium ions around 1445 and 1540 cm^{-1}, respectively, the density of the wafer, and the molar extinction coefficients published by Datka et al. [41]. The ^{27}Al MAS-NMR spectrum was measured on a Bruker DSX 400 spectrometer, using a 4 mm zirconia rotor and a spinning rate of 12 kHz. The resonance frequency for ^{27}Al was 104.2 MHz. A π/12 pulse was used, and the recycling delay was 250 msec. Each spectrum consisted of a minimum of 2400 scans. Aqueous $Al(NO_3)_3$ was used as an external standard ($\delta = 0$ ppm).

Transmission electron microscopy (TEM) images were obtained with a JEOL 100CX microscope using a 100 kV acceleration voltage. The samples were prepared by applying a slurry of the catalyst in ethanol on a graphene coated, 200 mesh copper grid. The slurry was sonicated for 15 min prior to applying to the sample grid. The Pt particle size distribution was determined based on these micrographs.

2.3. In-situ ATR IR spectroscopy

All spectra were acquired using a Thermo-Nicolet 8700 FT-IR spectrometer with an MCT/A detector. Each spectrum was collected with a resolution of 4 cm^{-1} and 32 scans. A commercial heated flow-through ATR cell from Pike Technologies (catalogue number: 022–5210) was used for the experiments. It contained an Internal Reflectance Element (IRE) (ZnSe crystal, 45°, 80 × 10 × 3 mm, Pike Technologies). During the experiments, a spectrum was collected every 30 s. To coat the IRE with a catalyst layer that was thicker than the penetration depth of the IR beam, a suspension of 12.5 mg of catalyst in 10 mL of ultrapure water was prepared and sonicated for 30 min. The catalyst was deposited onto the ZnSe crystal in layers. After each deposition step, the water in the layer was evaporated at 60 °C in an oven. The process was repeated until all of the suspension was deposited on the crystal.

For each experiment, 4 different feeds were prepared in separate bottles: ultrapure water degassed with He, an aqueous solution of 1 wt% of reactant (i.e. glycerol, sorbitol, and glucose) degassed with He, ultra-pure water saturated with O_2 gas, and ultrapure water saturated with H_2 gas. These feeds are henceforth referred to as H_2O, reactant (i.e. glycerol, sorbitol, and glucose), $O_2(H_2O)$, and $H_2(H_2O)$, respectively. The solutions were saturated with the respective gases for at least 4 h prior to the start of each experiment. The feed solutions were pumped through the ATR-IR cell with an Agilent 1200, quaternary HPLC pump at a flow rate of 5.0 mL/min. The catalyst bed in the ATR cell was stabilized in a flow of degassed ultrapure water (5.0 mL/min) for 3 h prior to the start of an experiment until the system reached a mechanically stable state of the catalyst bed (usually less than 1 h, as observed by reaching a constant absorbance spectrum). To remove adsorbed carbonaceous contaminants from the catalyst, H_2O, $O_2(H_2O)$, and $H_2(H_2O)$ were flowed through the ATR IR cell for sequential 30 min intervals.[30] This cleaning procedure was repeated two times (Fig. 1). The background was collected during the last minute of the cleaning procedure, prior to the start of the experiment. During the experiments, different feed solutions flowed through the cell (Fig. 1). A typical experiment consisted of 30 min of reactant solution, followed by H_2O, and $O_2(H_2O)$. Separate experiments were performed with glycerol, sorbitol, and glucose solutions as reactants at temperatures of 24, 50, and 72 °C. Thermo Fisher Scientific Inc. GRAMS 9.1 was used to analyze and integrate the peaks in the spectra. The peak of linearly bound CO was integrated from ca. 2060 to 1870 cm^{-1}, and the one bridging CO on Pt peak was integrated from ca. 1870 to 1734 cm^{-1}.

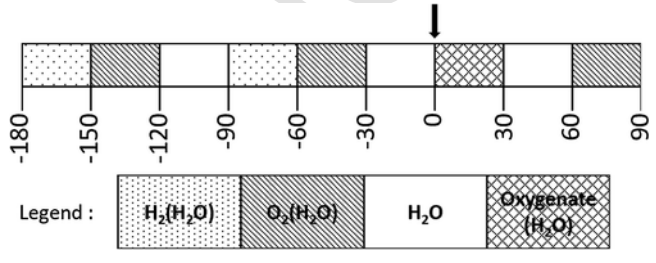

Fig. 1. Flow periods used during the cleaning of the catalyst and the conversion of aqueous oxygenate solutions (including time scale in minutes).

2.4. NMR spectroscopy

γ-Al_2O_3 (250 mg) was impregnated with 5 mL of an aqueous $^{13}C_6$-glucose solution in a 20 mL scintillation vial. The concentration of glucose was adjusted to achieve a glucose loading of 1 wt%. The prepared slurry was subject to vortex mixing for 1 min and sonication for 10 min. This procedure was repeated 3 times. The resulting slurry mixture was dried under vacuum overnight. ^1H-^{13}C cross polarization (CP) NMR experiments were conducted on a 20 T Varian VNMRs system utilizing a 4 mm HXY probe operating in HX mode tuned to 213.6862 MHz. A linear ramp CP sequence was utilized with a ^1H $\pi/2$ pulse of 3.125 μs, a mixing time of 500 μs, and two phase pulse modulation (TPPM) decoupling with a decoupling field of 76923 Hz. A recycle delay of 8 s, a spinning speed of 15 kHz, and a constant temperature of 20 °C were used to collect 4844 transients. The time domain free induction decay was zero filled once and apodized with 50 Hz of Lorentzian broadening. The spectrum was referenced against tetramethylsilane (TMS) at 0 ppm.

3. Results

3.1. Catalyst characterization

The Pt/γ-Al_2O_3 catalyst used here was from the same batch that was used and characterized in more detail in a previous study [30]. The surface area and pore size distribution of Pt/γ-Al_2O_3 as determined by N_2 physisorption were in the expected range (Table S1). X-ray diffractions at $2\theta = 44.6°$ and 66.7° represented the (4 0 0) and (4 4 0) planes of the defective spinel structure of the γ-Al_2O_3 support [42]. The ^{27}Al MAS NMR spectrum contained two peaks at 7 and 63 ppm, which are attributed to octahedrally and tetrahedrally coordinated Al atoms. The integrals of these peaks showed that the sample contained 77% octahedrally coordinated Al and 23% tetrahedrally coordinated Al species, which is typical for γ-Al_2O_3 [43]. An average Pt size of 3 nm was determined by measuring 177 Pt particles in TEM micrographs. IR spectra of adsorbed pyridine exhibited peaks from the ν_{19b} mode at 1448 cm^{-1} and the ν_{8a} mode at 1613 cm^{-1} that are attributed to pyridine coordinated to Lewis acid sites. The concentration of Lewis acid sites was quantified as 18 μmol/g. However, the ν_{19b} mode of pyridine coordinated to Brønsted acid sites (i.e., pyridinium ions), which is commonly observed at ca. 1540 cm^{-1}, was absent [44].

3.2. Identification of surface species formed during APR of glycerol, sorbitol, and glucose

When Pt/γ-Al_2O_3 coated on a ZnSe crystal was placed in an in-situ ATR-IR cell and exposed to an aqueous glycerol solution (1 wt%), the resulting IR spectra contained two strong peaks at around 2017 and 1788 cm^{-1}, which are attributed to the stretching vibrations of linearly bound CO (CO_L) and bridging CO (CO_B) on the Pt surface, respectively (Fig. 2b) [11,30,45]. CO_L and CO_B were also formed from aqueous sorbitol (Fig. 3b) and glucose (Fig. 4b) solutions, but the corresponding peaks appeared at lower wavenumbers (Table S2). Over the course of each aqueous oxygenate solution flow (i.e., 30 min), these peaks gradually shifted to higher wavenumbers, respectively, due to increasing dipole-dipole interactions with increasing coverage [29].

The other peaks in Fig. 2b are all attributed to various modes of glycerol according to Colthup et al. (Table 1) [46]. No significant peaks that would indicate the presence of hydroxyacetone or glyceraldehyde were observed during any flow period of this experiment. Differences between the peaks from glycerol in the presence of Pt/γ-Al_2O_3 (Fig. 2b) and its absence (Fig. 2a) in terms of positions and shapes were marginal, and the peaks rapidly declined during the subsequent H_2O flow

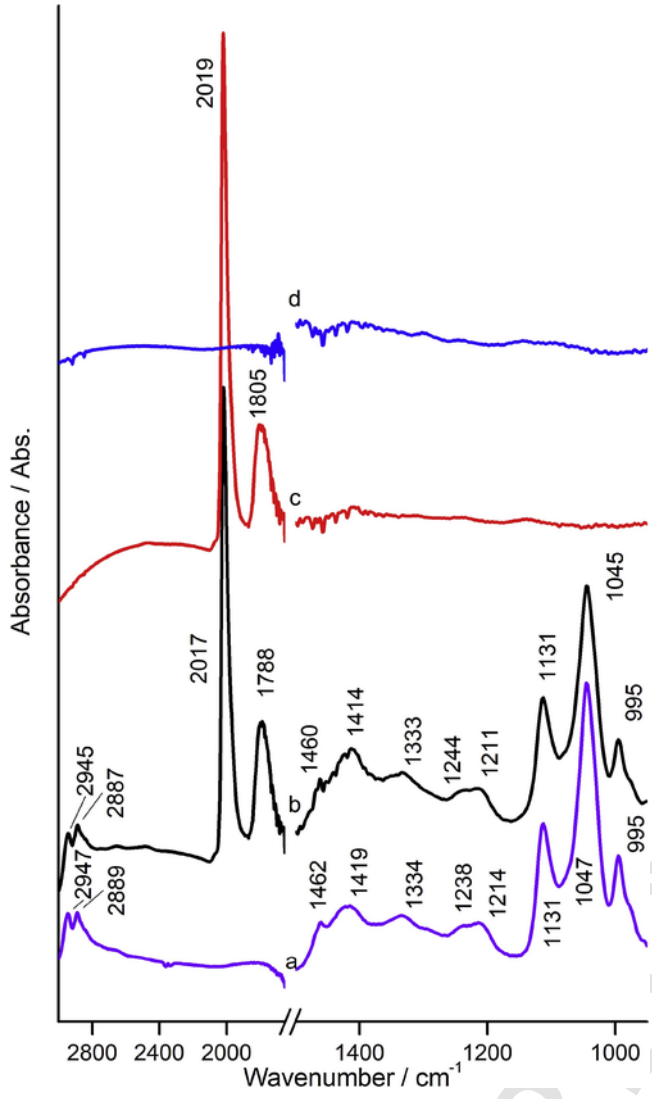

Fig. 2. ATR-IR spectra of 1 wt% glycerol in water in the absence of a catalyst (trace a), and surface species formed on a Pt/γ-Al_2O_3 catalyst layer: b) during 1 wt% glycerol in water flow; c) subsequent H_2O flow; d) subsequent $O_2(H_2O)$ flow. All of the spectra were taken after 10 min of the respective flow period.

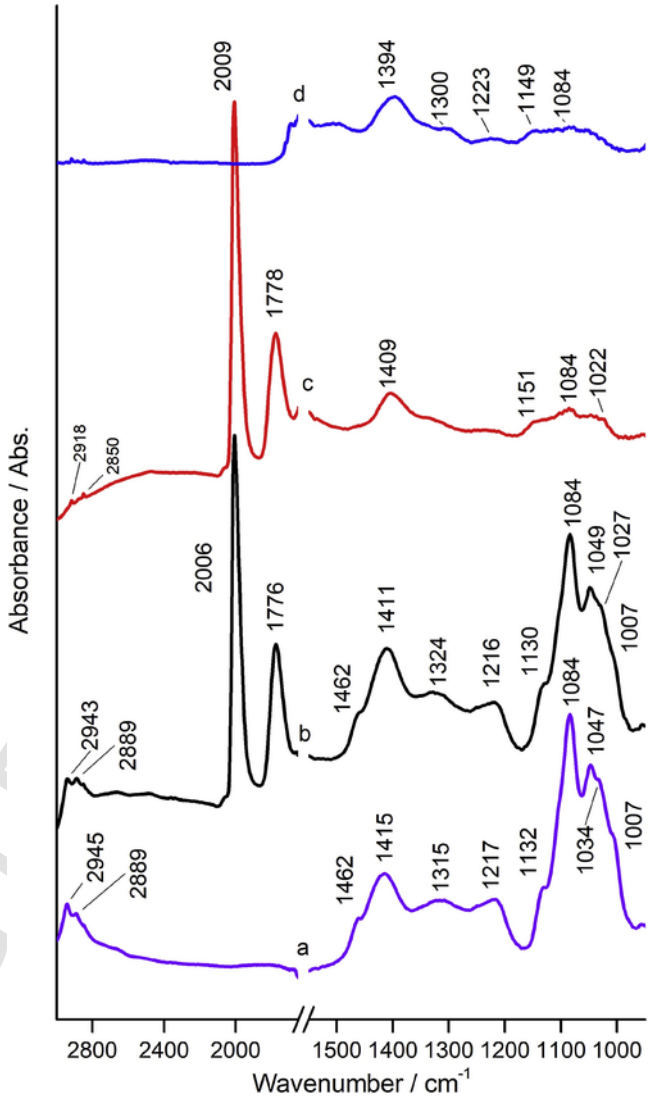

Fig. 3. ATR-IR spectra of 1 wt% sorbitol in water in the absence of a catalyst (trace a), and surface species formed on a Pt/γ-Al_2O_3 catalyst layer: b) during 1 wt% sorbitol in water flow; c) subsequent H_2O flow; d) subsequent $O_2(H_2O)$ flow. All of the spectra were taken after 10 min of the respective flow period.

(Fig. S1). This indicates that most of the intensity of the glycerol peaks in the range from 900 to 1600 cm^{-1} comes from the liquid phase and that the peaks from glycerol in water may obscure smaller peaks of other surface species that might be present on Pt/γ-Al_2O_3.

During the H_2O flow, a significant negative peak was observed above 2600 cm^{-1}, which is attributed to the νOH mode of water. It is suggested that residual surface hydrogen from the decomposition of glycerol interfered with the formation of a H_2O bilayer on Pt particles (Fig. 2c) [30]. This feature disappeared when the catalyst was exposed to an $O_2(H_2O)$ flow because adsorbed H atoms were oxidized by O_2 [30]. Moreover, the peaks of CO_L and CO_B disappeared during $O_2(H_2O)$ flow (Fig. 2d), which is attributed to the oxidation of these species. Upon exposure to $O_2(H_2O)$, new peaks were observed at 1614, 1493, and 1394 cm^{-1} (Fig. S2) that are completely removed by the end of the $O_2(H_2O)$ flow period ((Fig. 2d). In a reference experiment, CO_2 saturated H_2O was flowed over Pt/γ-Al_2O_3, and the peak positions of the resulting carbonate surface species matched those observed during oxidation of adsorbed CO (Fig. S4). The rapid removal of adsorbed CO and formation of carbonates was also observed during the $O_2(H_2O)$ flow periods in experiments with sorbitol (Fig. 3d) and glucose solutions (Fig. 4d).

When the aqueous sorbitol feed was flowed into the cell, there were multiple peaks between 950 and 1550 cm^{-1} that are attributed to both adsorbed sorbitol and sorbitol in the aqueous phase (Fig. 3b). In contrast to the aqueous glycerol feed (Fig. 2b), which exhibited two distinct νCO modes at 1131 and 1045 cm^{-1}, the νCO modes of sorbitol gave rise to several peaks at 1130, 1084, 1049 and 1027 cm^{-1}, which are attributed to primary and secondary alcohols of sorbitol interacting with H_2O and Pt/γ-Al_2O_3 in diverse ways (Fig. 3b). After 30 min of H_2O flow, peaks of the δOH, two νCO modes of sorbitol-derived surface species remained at 1409, 1084, and 1022 cm^{-1}, respectively. Additional peaks remained at 2918, 2850, and 1151 cm^{-1} and are attributed to the $\nu_{asym}CH_2$, $\nu_{sym}CH_2$, and νCO modes of surface alkoxy species on the Al_2O_3 support.[36] However, the νCH_2 bands were very low in intensity. The remaining δOH and νCO peaks at the end of the subsequent $O_2(H_2O)$ flow period (Fig. 3d) indicated that certain irreversibly adsorbed surface species cannot be entirely removed by O_2.

The spectrum of 1 wt% glucose in aqueous solution exhibited strong bands in the 1160–990 cm^{-1} region involving νCO modes of COH and COC groups and multiple moderately intense bands in the 1460-1200 cm^{-1} region attributed to CH_2 deformation (δCH_2), and CH_2 wag-

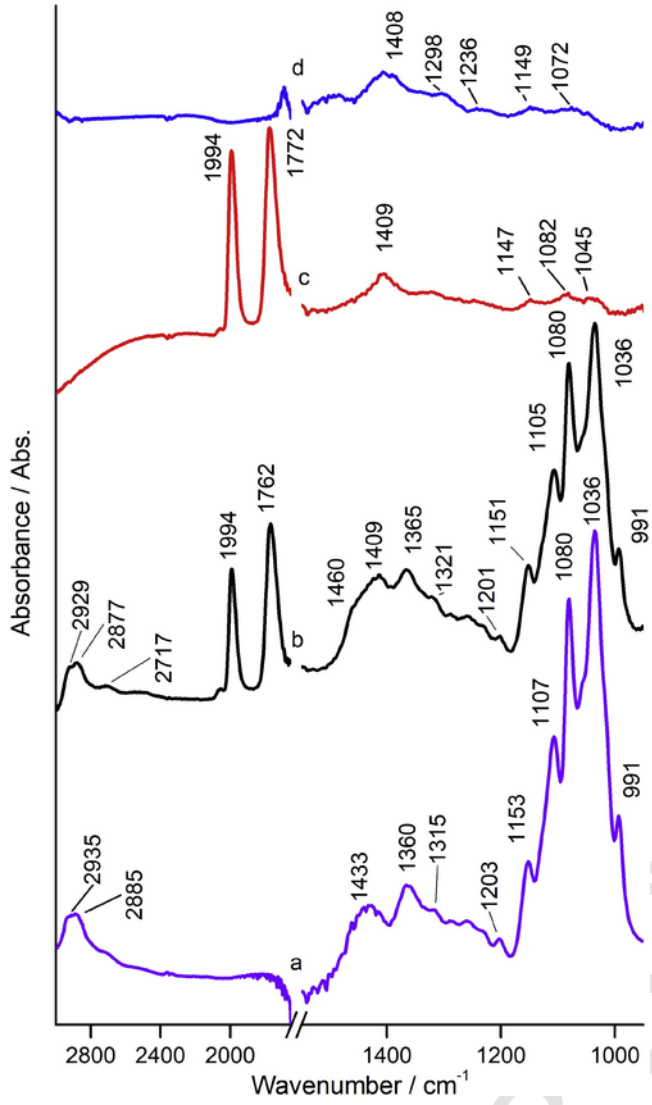

Fig. 4. ATR-IR spectra of 1 wt% glucose in water in the absence of a catalyst (trace a), and surface species formed on a Pt/γ-Al_2O_3 catalyst layer: b) during 1 wt% glucose in water flow; c) subsequent H_2O flow; d) subsequent $O_2(H_2O)$ flow. All of the spectra were taken after 10 min of the respective flow period.

ging, and OH in-plane deformation (δOH) (Fig. 4a). While this region of the spectrum is certain very convoluted, it appears that a new peak arises at 1409 cm^{-1} indicating that some of the glucose chemisorbs on the catalyst in a way that significantly alters the geometric or electronic structure of the molecule. One possible transformation is ring opening of the abundant hemi-acetal form of glucose. As a reference, the ^{13}C CP MAS NMR spectrum of glucose on γ-Al_2O_3 was obtained (Fig. 5). No clear peak of a free carbonyl group was observed in the region of 190–205 ppm showing that glucose predominantly adsorbs on γ-Al_2O_3 in a cyclic form. However, it is possible that Pt particles induced ring-opening of glucose as observed in another study under UHV condition [47]. After 30 min of H_2O flow, peaks of the δOH and the two νCO modes of glucose-derived surface species remained at 1409, 1082, and 1045 cm^{-1}, respectively. An additional peak at 1147 cm^{-1} is attributed to νCO modes of surface alkoxy species on the Al_2O_3 support. The intensity in the 1460-1200 cm^{-1} region decreased markedly in the first minute of the H_2O flow period (Fig. S3), but residual peaks remained until the end of the 30 min period.

3.3. Evolution of surface species at different temperatures

The influence of the reaction temperature on the formation of surface intermediates from glycerol, sorbitol, and glucose was investigated based on the IR spectra obtained after feeding the aqueous oxygenate solution for 30 min, followed by 10 min of pure H_2O (Fig. 6). This approach was chosen to reduce the spectral contribution of the aqueous oxygenate solutions. Glycerol reforming at 24, and 50 °C only resulted in very weak features that might be peaks of persistent surface species (Fig. 6a and b). Specifically, the potential νCO peaks at 1140 and 1060 cm^{-1} could indicate the presence of alkoxy species on the γ-Al_2O_3 support. During the experiment at 72 °C, broad peaks appeared around 1300 and 1061 cm^{-1}, which can be attributed to CH_2 twisting mode and the νCO modes of adsorbed alkoxy species at the elevated temperature (Fig. 6c) [11].

Prominent surface species were formed from the interaction of sorbitol with the catalyst at all temperature studied (Fig. 6d–f). Specifically, the broad peaks of νCO modes existed between 1000 and 1200 cm^{-1}, and the δOH peak at 1403 cm^{-1} was observed due to the existence of diverse alcohol and alkoxy groups. The broad peaks in this region indicate that many types of alcohol-derived surface species are present, which may include surface-bound decomposition products from sorbitol. At 72 °C, a broad peak around 1300 cm^{-1}, which can be attributed to δCH_2 modes, and a peak at 1147 cm^{-1} attributed to the νCO mode of surface alkoxy species were observed (Fig. 6f). The intensity of the νCO at 1147 cm^{-1} of surface intermediates from sorbitol at 72 °C was noticeably lower compared to 24, and 50 °C, which might indicate that primary alcohol groups of surface species are preferentially dehydrogenated or dehydrated.

Interestingly, glucose formed similar surface species as sorbitol with peaks of a δOH and three νCO modes at 1403, 1146, 1074 and 1057 cm^{-1} (Fig. 6g–i). As for sorbitol, the intensity of the νCO mode at 1022 cm^{-1} was lower at 72 °C (Fig. 6i). The most prominent difference at 72 °C was the noticeably broader feature in the δCH_2 and δCH_3 region around 1300 cm^{-1}.

Table 1
Vibrational modes of reactant solution over the empty ZnSe crystal and aqueous reactant solution interacting with the catalyst layer.

	1 wt% Glycerol in H_2O / cm^{-1}	1 wt% Glycerol over Pt/γ-Al_2O_3 / cm^{-1}	Δ/ cm^{-1}	1 wt% Sorbitol in H_2O / cm^{-1}	1 wt% Sorbitol over Pt/γ-Al_2O_3 / cm^{-1}	Δ/ cm^{-1}	1 wt% Glucose in H_2O / cm-1	1 wt% Glucose over Pt/γ-Al_2O_3 / cm^{-1}	Δ/ cm^{-1}
$\nu_{asym}CH_2$	2947	2945	−2	2945	2943	−2	2935	2929	−4
$\nu_{sym}CH_2$	2889	2887	−2	2889	2889	0	2885	2877	−8
δCH_2	1462	1460	−2	1462	1462	0		1460	
δOH	1419	1414	−5	1415	1411	−4	1433	1409	−24
δCH	1334	1333	−1	1315	1324	9	1315	1321	6
CH_2 wag	1214	1211	−3	1217	1216	−1	1203	1201	−2
unknown	x	x		1132	1130	−2	1153	1151	−2
νCO 2°	1131	1131	0	1084	1084	0	1080	1080	0
νCO 1°	1047	1045	−2	1047	1049	2	1036	1036	0
CH_2 rock	995	995	0	1007	1007	0	991	991	0

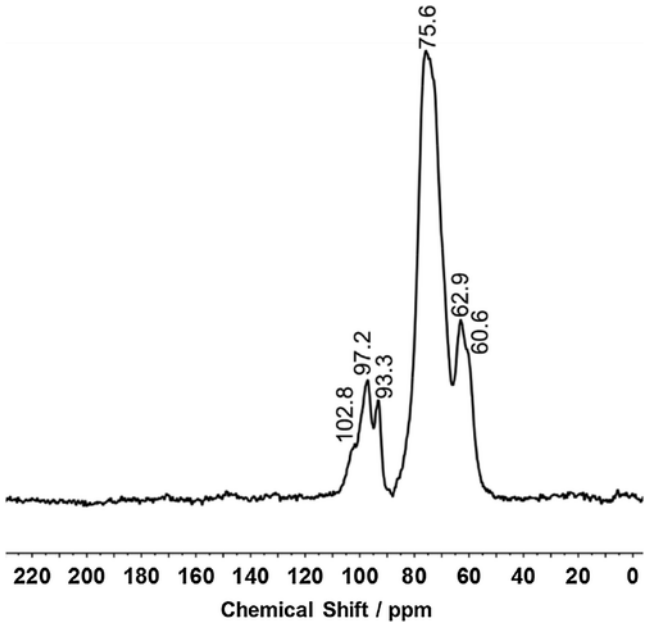

Fig. 5. ^{13}C CP MAS NMR spectrum of $^{13}C_6$-glucose impregnated on γ-Al_2O_3.

3.4. Rates of CO formation and conversion starting from glycerol, sorbitol, and glucose

The frequencies of νCO modes of adsorbed CO after 1 min of exposure to aqueous oxygenates decreased based on the source of CO in the order glycerol > sorbitol > glucose (Fig. 7). It is suggested that fragments from the larger oxygenates prevent dipole-dipole interactions and the associated blue-shift of the νCO mode. Interestingly, the νCO_B peak from glucose clearly contained two contributions at 1776 and 1751 cm^{-1} (Fig. 7c). This could be due to the presence of domains in which dipole-dipole interactions can develop to different extents. After 2 min of exposure to glucose the different contributions to the CO_B peak were no longer clearly resolved (Fig. 7c*).

The integrals of the CO_L and CO_B bands observed in Fig. 7 continuously changed during aqueous reforming of glycerol, sorbitol, and glucose. The rates of formation and conversion of CO_L and CO_B as well as the abundance of these species in different experiments were investigated based on the integrals of the respective peaks (Figs. 8–10). In all reactions studied here, CO_L and CO_B were formed when the aqueous oxygenate solution was flowed through the cell for 30 min. The conversion of glycerol at room temperature resulted in the largest integrated area of the CO_L, which was 1.5 and 4.7 times higher than the integrated area of CO_L from sorbitol and glucose, respectively (Fig. 8a). Fig. 8b shows that the highest area for CO_B was reached after 6 min and 9 min during glycerol and sorbitol flow period, respectively, followed by a gradual and apparently linear decrease throughout the oxygenate flow and the following H_2O flow period. The intensity of the CO_L peaks formed from glycerol and sorbitol remained approximately constant during the H_2O flow period (Fig. 8a).

When glucose was fed at 24 °C, CO_B and to a lesser extent CO_L kept accumulating over the entire glucose flow period (Fig. 8). After 30 min, the coverage of CO_B from glucose was 15% higher than the maximum coverage of CO_B from sorbitol (Fig. 8b). Without a continued supply of reactant during the H_2O flow period, CO_B produced from glucose declined at a similar rate as CO_B from the other oxygenates. Surprisingly, in case of glucose, the intensity of the CO_L band continueously increased in the absence of reactants in the feed during H_2O flow period. After 30 min of H_2O flow, it had increased by 40% compared to the

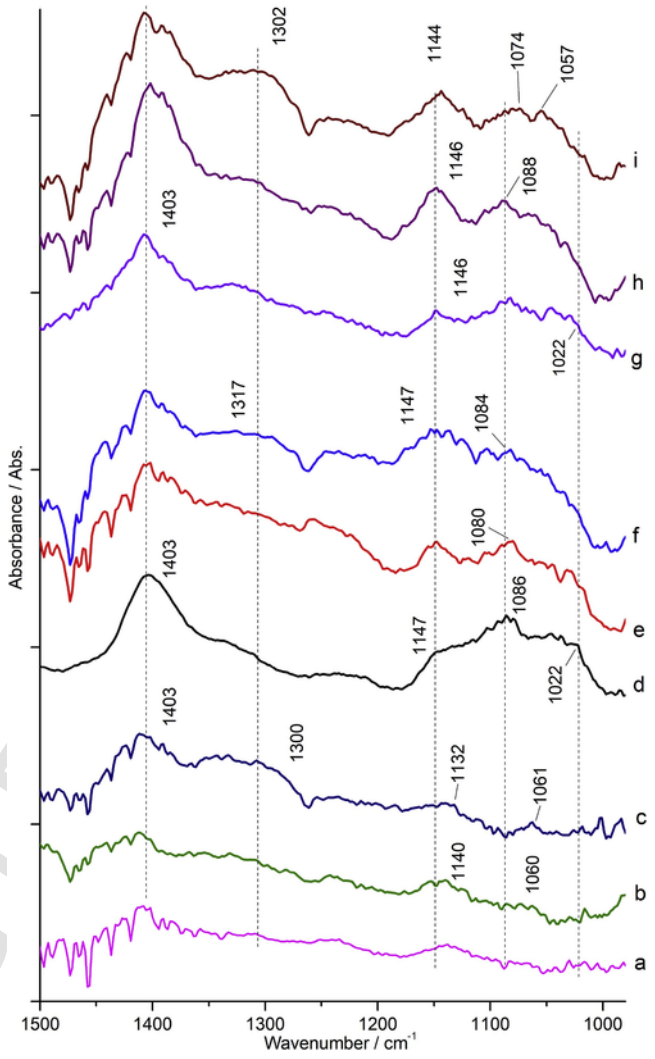

Fig. 6. ATR-IR spectra during the H_2O flow period after exposure of Pt/γ-Al_2O_3 to aqueous oxygenate solutions: Glycerol conversion at a) 24 °C, b) 50 °C, c) 72 °C (c); sorbitol conversion at d) 24 °C, e) 50 °C, f) 72 °C; glucose conversion at g) 24 °C, h) 50 °C, i) 72 °C. All of the spectra were taken after 10 min of their H_2O flow period.

CO_L band after the aqueous glucose flow (Fig. 8a). Fig. S5 shows that the increase in the intensity of the CO_L band coincided with a decrease of the peaks corresponding to the νCO mode of adsorbed glucose, which indicates that a reduction in the density of glucose on the surface allows for the production of additional CO_L. The ratios of the integral of the CO_L to CO_B peaks from glycerol and sorbitol were approximately 2 at the end of the oxygenate flow period. In contrast, a much smaller CO_L/CO_B ratio of 0.57 was observed after 30 min of aqueous glucose flow. Once $O_2(H_2O)$ water was flowed through the cell both bands of adsorbed CO disappeared rapidly, indicating fast oxidation of adsorbed CO to CO_2 or the corresponding carbonates at each reaction temperature (Figs. 8–10).

The evolution of the integrated regions of CO_L and CO_B during APR at 50 °C showed similar trends compared to the experiments at 24 °C. The increased reaction temperature led to an increase in the maximum coverage of CO_L during the conversion of sorbitol and glucose (Fig. 9a). Likewise, the maximum CO_B coverage from glucose increased (Fig. 9b). The maximum coverage of CO_B was observed after 6.2 and 6.7 min during the conversion of glycerol and sorbitol, respectively, followed by a gradual and almost linear decline that extended throughout the rest of the aqueous reactant flow until the end of the H_2O flow period. Interestingly, glucose produced as much CO_B as glycerol, with maxima

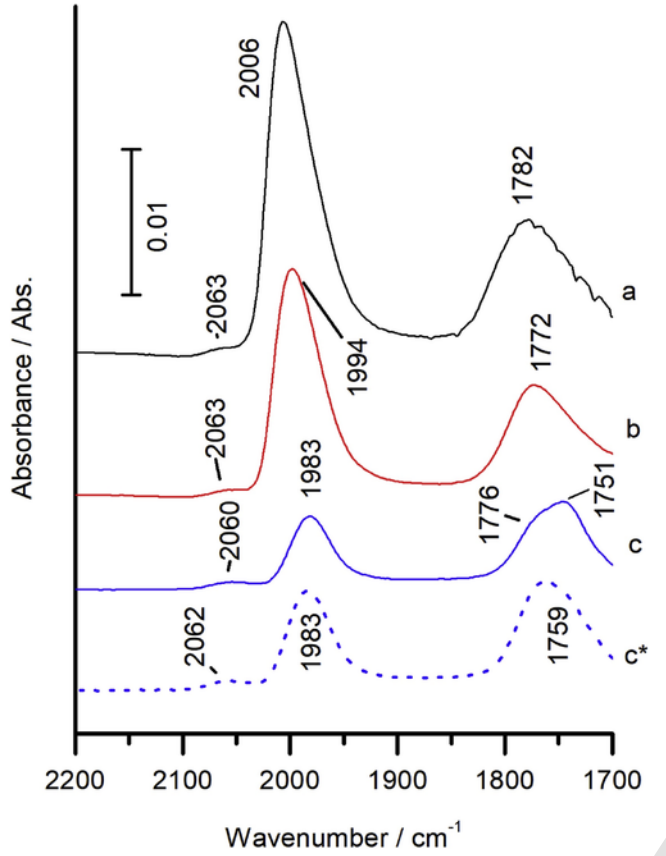

Fig. 7. Spectra of CO_L and CO_B formed on Pt/γ-Al_2O_3 taken after 1 min of exposure to a) glycerol, b) sorbitol, c) glucose; and c*) after 2 min of exposure to glucose. All spectra were taken at 24 °C.

of the integrated peak areas that were 25% larger than for the CO_B peak during the conversion and sorbitol. In contrast to the conversion of glycerol and sorbitol, the intensity of the CO_B peak from glucose gradually approached a constant value while the aqueous glucose solution was fed and decreased sharply at the beginning of the H_2O flow period. Then, the area of the CO_B peak showed the similar gradual decline as observed during the H_2O flow periods after conversion of glycerol and sorbitol.

At a reaction temperature of 72 °C, the maximum peak area of CO_L was higher than at 50 °C, and the peak area of CO_L decreased during the H_2O flow period (Fig. 10a). The area of the CO_B peak exhibited a similar behavior for all the reactants with maxima after 0.6, 2.5, and 4.5 min for glycerol, sorbitol, and glucose, respectively (Fig. 10b). Then, it decreased sharply even in the presence of the reactants. During the H_2O flow period, the observed rate of CO_B conversion became slower. In fact, it was slower than at 24 and 50 °C.

The initial changes of the peak areas with respect to time (proportional to the rate of formation) of CO_L and CO_B at the initial contact of different reactants with the catalyst is plotted in Fig. 11. The initial rates of formation of both CO_L and CO_B were fastest during the conversion of glycerol. The rates of CO_L formation from all reactants increased to a similar extent with increasing temperature. The only exception was a sharp increase in the initial rate of formation of CO_L from glucose at 72 °C. The initial rate of CO_B formation changed less as the temperature increased. During the conversion of glycerol and sorbitol, it decreased slightly as the temperature increased from 24 to 50 °C, and then increased when the temperature increased further to 72 °C. The initial rate of CO_B formation from glucose showed a continuous increase, starting from a very low value at 24 °C.

4. Discussion

4.1. Surface species during APR of glycerol, sorbitol, and glucose

The three primary steps in the mechanism of APR of polyols are dehydrogenation, decarbonylation, and water-gas-shift (WGS, i.e., $CO + H_2O \rightarrow CO_2 + H_2$) (Scheme 1) [11,17]. The key intermediate, adsorbed CO, is formed through a sequence of dehydrogenation of a primary alcohol group to an aldehyde and decarbonylation of the aldehyde to forming CO [11]. Dehydrogenation of a secondary alcohol group results in the formation of a ketone, which cannot be decarbonylated directly like an aldehyde [38]. The dissociation of water during the WGS reaction is generally assumed to be the slowest step in APR [5,14,17]. Many surface studies observed CO bound to one Pt atom (linearly bound, CO_L) or two Pt atoms (bridging, CO_B) and H atoms as dominant surface species during APR reactions over Pt-based catalysts 1730]. An ATR-IR spectroscopy study of methanol reforming over Pt/γ-Al_2O_3 in vapor and liquid phase showed that the surface coverage of CO is lower in the liquid environment, which could be due to weaker binding or competitive adsorption of other species 17]. In particular, dissociatively adsorbed hydrogen reduces the number of surface sites that are available for activating methanol.

Several researchers proposed the formation of dehydrogenated polyols, such as $C_xO_xH_{2x}$, on supported Pt particles as intermediates of APR [4,48], but the presence of these species is typically inferred from

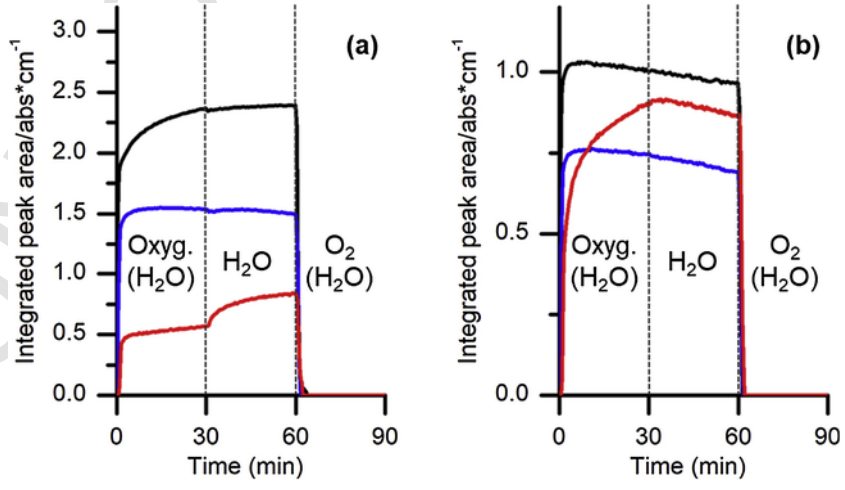

Fig. 8. The integrated peak area of the νCO_L mode (a) and the νCO_B mode (b) as a function of time and type of reactant at 24 °C, — glycerol, — sorbitol, and — glucose.

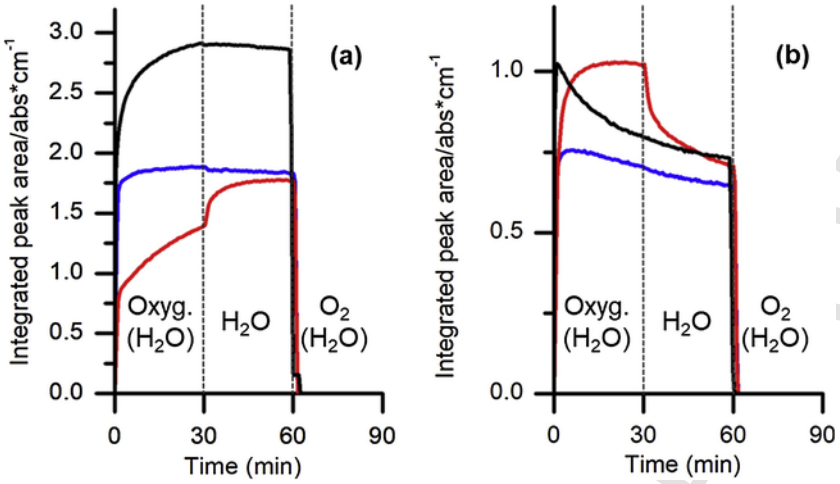

Fig. 9. The integrated peak area of the νCO_L mode (a) and the νCO_B mode (b) as a function of time and type of reactant at 50 °C, — glycerol, — sorbitol, and — glucose.

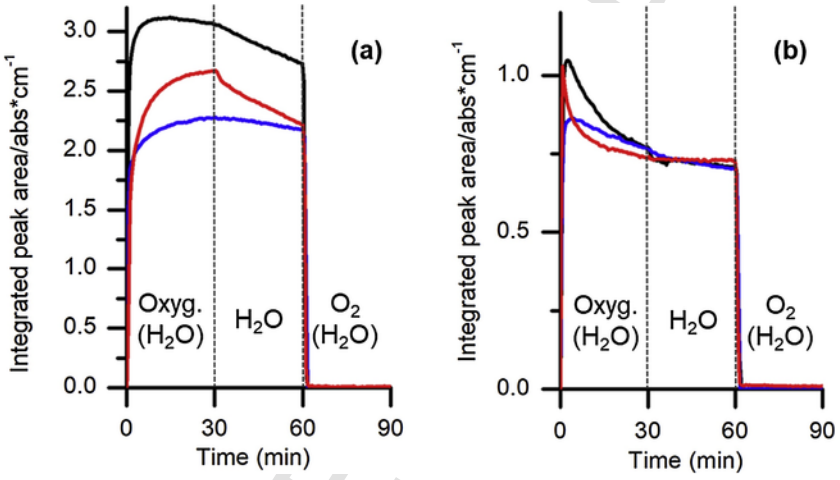

Fig. 10. The integrated peak area of the νCO_L mode (a) and the νCO_B mode (b) as a function of time and type of reactant at 72 °C, — glycerol, — sorbitol, and — glucose.

indirect evidence rather than direct spectroscopic detection [49]. A study of electrochemical glycerol oxidation in acidic media used IR spectroscopy, HPLC analysis, and DFT calculations to show that glycerol binds to Pt (111) as a bidentate $C_3O_3H_6$ intermediate, which can be converted to glyceraldehyde, dihydroxyacetone, and glyceric acid [50]. On Pt (100), a monodentate surface species is formed that involves a Pt-C bond with a primary carbon atom. Glyceraldehyde is the main product from this species. In addition, the presence of a strongly adsorbed surface species other than CO was inferred.

All oxygenates used in our study produced CO_L and CO_B as dominant surface species, but the abundance of these species varied between oxygenates and as a function of the reaction temperature. It is well-known that the size of the Pt particles has a strong influence on the distribution of CO_L and CO_B [51,52]. For example, it was shown that Pt particles of a minimum size are required before CO_B can be formed, indicating that this species is preferentially formed on terrace sites [53]. All of our experiments were conducted with the same of the size of Pt particles supported on γ-Al_2O_3, and it is highly unlikely that the different feedstocks significantly change the size of the particles during the APR at 24–72 °C. Therefore, any change in the abundance of CO species should be due to the surface reactions of different reactants and the resulting co-adsorbed surface species that compete with CO for specific active sites. The relative abundance of CO_B compared to CO_L was higher than in previous studies, in which CO was adsorbed on Pt/γ-Al_2O_3 in the presence and absence of water, which might be affected by co-adsorbed species, the size of the Pt particles, and solvent effects [29,54]. The CO_B to CO_L ratio in our study was strongly affected by the nature of the reactant, with values of 0.42, 0.49, and 1.6 for glycerol, sorbitol, and glucose, respectively, after 30 min of exposure to the aqueous oxygenate solution at 24 °C. In particular the uptake of CO_L after 30 min at 24 and 50 °C, decreased markedly in the order glycerol > sorbitol > glucose. These observations indicate that sites at which CO_L can be formed are preferentially blocked by co-adsorbed species. It is important to note that these species may be directly bound to the Pt sites or adjacent support sites. Since the conversion of glucose to CO requires opening the cyclic hemiacetal as the first step, it is plausible that CO formation from glucose proceeds more slowly. Moreover, unreactive surface species can be formed in parallel and reduce the number of available sites for CO formation. The formation of additional CO_L from residual adsorbed glucose during H_2O flow (Figs. 8a and 9a) shows that a reduced density of surface species provides the required space for the decomposition of glucose to CO_L. It is recognized that APR of sorbitol, which contains six carbon atoms like glucose, also occurs via an aldose as an intermediate. However, it appears that the decarbonylation of the aldose intermediate is fast relative to the formation of a hemiacetal, resulting in a faster rate of CO formation from sorbitol. This is in agreement with lack of glucose in the product stream during APR of sorbitol over Pt/Al_2O_3 [7].

In all of our experiments, the frequency of the νCO vibrations of CO_L and CO_B increased with increasing coverage. Previous studies have

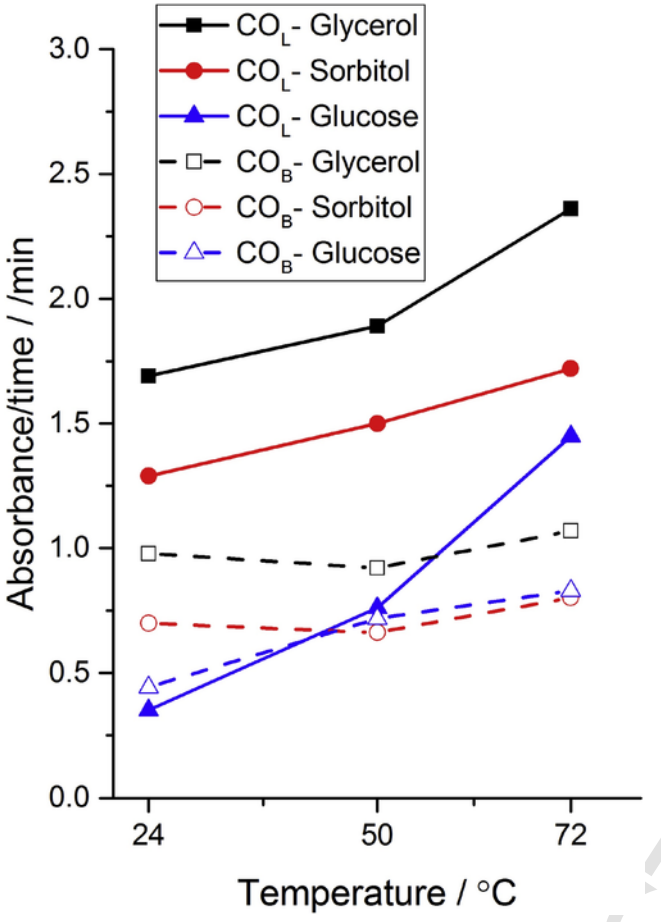

Fig. 11. Initial changes of the peak areas with respect to time (proportional to the rate of formation) of CO_L and CO_B based on peak areas after 1 min of exposure to different reactants at different temperatures.

attributed similar observations to two different phenomena. It is well-known that adsorbed CO molecules have dipole-dipole interactions with their neighbors, which results in an increase of the vibrational frequency with increasing density of CO on the surface [28,55]. Alternatively, electronic effects can explain the shifts of νCO peaks. Specifically, it has been proposed that CO_L and CO_B initially form at undercoordinated Pt sites at edges and kinks [56]. Once these sites are occupied, more CO_L and CO_B also form on terrace sites that consist of more coordinated metal Pt atoms, which results in a higher frequency. Based on this argument, the increasing νCO frequency in our study (Table S2) could indicate that decarbonylation reactions preferentially occur at edge and kink sites and that the resulting CO species are migrating to terrace sites. This would be consistent with a DFT study that found a higher activity for decomposition of ethylene glycol on Pt(211) compared to Pt(111) [12]. However, the present data does not allow for deconvoluting the extent of such migration processes from the impact of dipole-dipole interactions.

The conversion of glucose at 24 °C led to the formation of two distinct CO_B species at 1776 and 1751 cm^{-1} (Fig. 7). It is well-known that co-adsorbed surface species can isolate CO on Pt in different environments. For example, when CO is co-adsorbed with less than one monolayer of H_2O, islands containing pure CO and a mixture of CO and H_2O, respectively, can be formed [[57–59]. Due to dipole-dipole interactions, CO_B in islands of pure CO has a higher vibrational frequency. In the present study, the existence of distinct CO_B peaks during APR of glucose can be attributed to the formation of different domains on the surface. While some domains contain sizable ensembles of CO molecules with dipole-dipole interactions, others contain CO species that are relatively isolated by co-adsorbed glucose or glucose-derived oxygenates. The latter domains can be attributed to the contribution with the lower νCO frequency, which was also lower than the νCO frequencies of CO_B from glycerol and sorbitol. When the CO coverage increased the different contributions to the CO_B were no longer resolved. Furthermore, the formation of distinct islands of CO formed from glycerol and sorbitol was not observed. Thus, it is suggested that cyclic forms of glucose are capable of adsorbing on or adjacent to Pt particles to block a significant fraction of the metal sites.

γ-Al_2O_3 is a useful support to stabilize Pt nanoparticles. However, it also provides a high surface area with adsorption sites for oxygenates. A study of polyol adsorption on hydrated alumina showed that incrased adsorption with an increasing number of vicial alcohol groups, in particular when they are present in the threo configuration [59]. Copeland et al. used a combination of FT-IR spectroscopy and DFT calculations to reveal that glycerol and 1,3-propanediol form a multidentate surface species on γ-A_2O_3, in which one of the primary alcohol groups forms a bridging alkoxy bond to a Lewis acid site (ν = 1125 cm^{-1}) [36]. The other primary alcohol group coordinates to the same Lewis acid site without dissociating (ν = 1083 cm^{-1}), while the secondary alcohol group in glycerol can hydrogen bond to a basic surface oxygen atom (ν = 1151 cm^{-1}). These multidentate surface species are bound sufficiently strongly to effectively outcompete water for surface sites [60]. In contrast, ethylene glycol and 1,2-propanediol only form alkoxy bonds to the Lewis acidic sites of γ-Al_2O_3 after removal of coadsorbed water in vacuum because the stability of bidentate surface species from these molecules is reduced due to strain.

During the H_2O flow period after exposure to an aqueous glycerol solution, only very weak features remained at 1140 and 1060 cm^{-1} (Fig. 6a–c), which might be νCO modes of a small amount of alkoxy species on surface. This region of the spectrum was different from the adsorption of glycerol on pure alumina in Copeland's work [36], which would imply the presence of different alkoxy species, such as products of dehydration or C—C cleavage. When the temperature was increased to 72 °C a broad δCH_2 deformation peak indiated the formation of a new unknown surface species (Fig. 6c). It is suggested that dehydration and possibly oligomerization reactions lead to the formation of surface species containing alkyl groups.

During the conversion of sorbitol and glucose, much stronger residual νCO peaks were observed between 1160–1030 cm^{-1} after the aqueous oxygenate solutions were replaced by pure water and water saturated with O_2 (Figs. 3 and 4). This indicates the presence of strongly chemisorbed alkoxy species. The fact that these species remained on the catalyst during the O_2 (H_2O) flow period strongly indicates that they are on the Al_2O_3 support rather than the Pt particles where O_2 is known to oxidize and remove organic surface species [61]. The significant breadths of the νCO peaks can be explained with distributions of nature of surface alkoxy species and the strength of the Lewis acid sites involved in their formation. Notably, the spectra of surface species from sorbitol and glucose that remained during the H_2O flow period were very similar at each temperature (Fig. 6). Thus, there seems to be a reaction path to common surface species from these oxygenates. The dehydrogenation of sorbitol to an aldose, such as glucose, is a necessary step in the APR mechanism, but glucose could also be hydrogenated to sorbitol with surface hydrogen that is formed by reforming other molecules. Considering that the ^{13}C CP MAS NMR spectrum of glucose adsorbed on γ-Al_2O_3 (Fig. 5) did not contain the characteristic resonance of the aldehyde group in the open-chain form of glucose, we speculate that C_6 sugars in one or more cyclic hemiacetal forms are common surface species on alumina during the conversion of sorbitol and glucose. The increased accumulation of such surface species with increasing number of oxygen-based functional groups is consistent with results extrapolated from previous studies (vide supra) 59,60. The rela-

tive rigidity of the alcohol groups on the cyclic forms of sugars likely has a strong influence on the formation of specific species, but the exact nature of these species is beyond the scope of this work.

The extent to which carbonaceous surface species on the support affect APR catalysts strongly depends on their location relative to the Pt particles, which are generally considered to be the active sites for all essential steps in APR (i.e., dehydrogenation, decarbonylation, and water-gas shift). Deposits at a sufficient distance will be spectators and can help to protect the alumina support against hydrolytic decay [62]. In contrast, surface species close to the metal-support-interface can be converted via bifunctional reaction paths or sterically block access to parts of the Pt particles. While the present data does not exclude the presence of spectator species at a distance from the Pt particles, several observations illustrate the likely participation of surface species at the metal-support-interface on the APR reaction. Most importantly, the rate of CO_L formation was affected much more strongly by the nature of the reactant than the rate of CO_B formation (Fig. 11). Considering the preference for CO_L formation on edge and kink sites and that such sites are more abundant near the metal-support interface, we suggest that these trends are caused by blockage of metal sites near the interface with the support. However, preferential blockage of edge and kink sites in other locations cannot be excluded based on the present data. In addition, the similarity of surface species formed from glucose and sorbitol implies that their precursors can be converted by metal catalyzed dehydrogenation or hydrogenated before they strongly bind to the support. Under such circumstances an enrichment of such surface species near the metal particles is plausible. The formation of additional CO_L from glucose during the H_2O flow periods at 24 and 50 °C also implies that a decreased density of surface species in the vicinity of edge and kink sites allows reactants to approach them in the right orientation for decarbonylation to occur. This effect was not observed at 72 °C, which is attributed to increased mobility or desorption of surface species. It should be mentioned that the kinetic diameter of glucose is 0.86 nm [63], whereas the average size of the Pt particles used here was 3 nm. Thus, it is conceivable that a substantial number of metal sites at the interface are blocked when a significant fraction of the support is bound with strongly adsorbed surface species from reactants like glucose.

4.2. Kinetics of conversion of oxygenates with different numbers of carbon atoms and structures

The selectivity for H_2 production during APR of oxygenates over a Pt/γ-Al_2O_3 at 225 and 265 °C decreases in the order methanol > ethylene glycol > glycerol > sorbitol > glucose [9]. Due to their abundance as building blocks of lignocellulosic biomass, glucose and other sugars are desirable feedstocks. Like other aldoses, glucose already contains an aldehyde group, which is required for the decarbonylation step in APR [11]. Thus, it is important to analyze the kinetics of different reaction steps within APR to identify the reason for the low selectivity to hydrogen. The rate of APR of methanol and ethylene glycol to H_2 and CO_2 was similar under kinetically controlled reaction conditions suggesting that C—C bond cleavage, which involves dehydrogenation and decarbonylation, is not rate-limiting for ethylene glycol APR [4]. Therefore, undesirable parallel reactions or the formation of unreactive surface species from larger oxygenates appear to be likely explanations for the reduced yields. While homogeneous decomposition of glucose can certainly play a role at typical reaction temperatures [7,8], our results also point to the relevance of its interactions with metal and Lewis acid sites on Pt/γ-Al_2O_3.

In agreement with previous studies [29,30], most of the CO on the surface was formed faster than the temporal resolution of our ATR IR cell, which is about 30 s. However, important differences were observed for the achievable coverage of each species and the formation rates of additional adsorbed CO molecules beyond this point. Specifically, the formation of CO_L was affected by the nature of the reactant much strongly than the formation of CO_B. At 24 °C, the CO_L coverage after 30 min of exposure to aqueous glucose, sorbitol, and glycerol solutions had the approximate ratios of 1: 2.6: 4.1 (Fig. 8a). These strong differences are attributed to increased blockage of edge and kink sites by larger and more strongly adsorbed surface species from sorbitol and glucose. As discussed above, many of these species likely reside at the metal-support interface. Davis et al. also indicated that ketones adsorb particularly strongly under comparable conditions [38]. The likelihood of forming a ketone by dehydrogenation of a polyol or sugar certainly increases with an increasing number of secondary alcohol groups in the reactant. While the formation of ketones may be significant in our study, the present data do not allow for detecting such species. It should be noted that the presence of such co-adsorbed surface species has been inferred before, but they are notoriously hard to detect [64]. One could also suggest that the intensities of the CO_L vibration are low due to a high rate, at which these species are converted in subsequent reactions, but the low yields of hydrogen from larger oxygenates like sorbitol and glucose in reactivity studies indicate that this is not the case [9]. While the formation of CO_B from glucose was also slower compared to the other oxygenates at 24 °C, the difference in coverage after 30 min was much less pronounced. This suggests that the formation of CO_B on terrace sites is less inhibited by co-adsorbed oxygenates. After 30 min, the CO_B coverage from glucose was higher than that from sorbitol at all temperatures (Figs. 8b, 9b and 10b). This is attributed to a more selective path to aldehydes by ring opening and subsequent decarbonylation from glucose, whereas the dehydrogenation of a secondary alcohol group in sorbitol yields a ketone that cannot be easily decarbonylated and might block Pt sites. Moreover, the complete decomposition of glucose would result in the same number of adsorbed CO species and fewer co-adsorbed hydrogen atoms compared to sorbitol.

The differences in the achievable coverage of CO_B and CO_L from different feedstocks became less pronounced with increasing temperature. This could be explained with facilitated desorption of co-adsorbed oxygenates. In addition, we speculate that glucose is increasingly present in the open-chain form at elevated temperature [65], which is the prerequisite for the decarbonylation of the aldehyde group. It is also suggested that the rate of the ring opening reaction explains the low rate of CO_L formation from glucose compared to other reactants over the entire temperature range (Fig. 11). The same trend was observed for the rates of CO_B at 24 °C, while CO_B was formed from sorbitol and glucose at the same rate at higher temperature. Thus, we speculate that the interactions of glucose with support sites at the perimeter of the metal particles interfere with the ring opening reaction and thus the formation of CO_L on kink or edge site, whereas at 50 °C and above glucose can rearrange more readily and undergo ring opening more freely on terrace sites. However, direct site blockage by cyclic forms of glucose or its reaction products may still be the reason for the lower H_2 yields from glucose compared to sorbitol at elevated temperature [7,9] even though the conversion of both reactants is expected to occur via the same open-chain aldose intermediate.

Glycerol exhibited the highest initial rate of CO_L and CO_B formation at all the temperatures studied (Fig. 11). This could be due to higher ratio of primary to secondary alcohol groups compared to sorbitol and glucose and the increased probability of dehydrogenation steps yielding aldehydes rather than ketones as a consequence thereof. However, competition for surface sites with co-adsorbed species could also play a role.

The conversion of adsorbed CO to CO_2 by water-gas shift is generally considered the slow part of APR [66]. Specifically, the dissociation of water to form a surface hydroxyl group has been proposed as rate limiting step [66]. It was shown that CO_B on Pt/Al_2O_3 can be converted

by this reaction at ambient temperature, while the reactivity of CO_L was much lower [30]. In the presence of O_2, both CO_L and CO_B are converted rapidly. Thus, the difference is the reactivity of these species has to be associated with the formation of reactive intermediates from water (likely a Pt−OH species) in the vicinity of adsorbed CO. He et al. demonstrated that atomic hydrogen binds strongly to the active sites for the water-gas shift reaction during APR leading to product inhibition [17]. In principle, the conversion of adsorbed CO by water-gas-shift should not be directly influenced by the reactant that CO was formed from. However, co-adsorbed surface species can restrict the required space for the formation of a hydroxyl groups adjacent to adsorbed CO or the reaction of the two to ultimately form CO_2.

In the present study, the conversion of some surface bound CO by water gas shift was observed in all experiments. The resulting CO_2 was not observed in the IR spectra, but evidence for adsorbed carbonates that are rapidly formed from CO_2 and water was obtained (Figs. 2–4). The surface coverage of CO_B from glycerol and sorbitol reached a maximum during the flow of the oxygenate solutions at each temperature and decreased at the same rate the rest of the oxygenate flow and the subsequent H_2O flow periods (Figs. 8b, 9b and 10b). The decrease of the CO_B coverage during the unchanged oxygenate flow cannot be explained with spontaneous desorption but rather indicates that these species are converted by water gas shift. The maximum shows that hydrogen atoms remain adsorbed on the surface and prevent the repopulation of sites that are vacated by conversion of CO_B, which is in agreement with previous studies [17,30]. The coverage of CO_L from glycerol and sorbitol during H_2O flow at 50 and 72 °C showed much smaller changes compared to CO_B. Based on this observation, it is concluded that the CO_B is predominantly located in an environment with sufficient space and activity for dissociation of water in the vicinity, whereas these conditions are not met for CO_L. This is consistent with the formation of CO_B on terrace sites (vide supra).

The concentration profiles for CO formed from glucose showed some unusual behavior. At 24 and 50 °C, additional CO_L was formed during the H_2O flow period (Figs. 8a and 9a). Typically, one would expect reduced coverage when the supply of a reactant is stopped. However, it is conceivable that the coverage of adsorbed reactants or intermediates on the surface can become so high that decomposition reactions like the formation of CO by decarbonylation are sterically inhibited. It is easy to imagine that such a crowding effect would affect a reaction like the conversion of the cyclic hemiacetal form of glucose to open chain form, which is a prerequisite for the decarbonylation reaction. While the formation of additional CO_L in a less crowded environment appears to be the main contribution at 24 °C, the sudden decline in CO_B coverage in the beginning of the H_2O flow period at 50 °C (Fig. 9b) indicates that some of CO might migrate to edge and kink sites to become CO_L once these sites become available when adsorbed oxygenates at the perimeter of the Pt particles are removed.

At 72 °C, the concentration of CO_B from all reactants declined more slowly during the H_2O flow (Fig. 10b), but the intensity of the CO_L peaks declined markedly during the experiments with glycerol and glucose (Fig. 10a). It is unlikely that the reactivity of CO_B would decrease with increasing temperature. Thus, our experiments suggest that the adsorbed CO can become sufficiently mobile to migrate from sites where it is linearly bound to terrace sites where it is bound as CO_B. Since the conversion of CO_B is compensated by this migration the intensity of the CO_B peak decreases at a reduced rate. It has been shown that water can induce the interchange between CO_B and CO_L [56].

5. Conclusions

At moderate reaction temperatures of 24–72 °C, different steps of APR of glycerol, sorbitol, and glucose over Pt/γ-Al_2O_3 occur at rates that are compatible with the temporal resolution of in-situ ATR-IR spectroscopy. The key intermediate for APR is CO that can be bound to one (linearly bound, CO_L) or two Pt atoms (bridging, CO_B). CO_B appears to be formed preferentially on terrace sites, while CO_L is more abundant on edge and kink sites. In addition, larger oxygenates like sorbitol and glucose tend to form strongly adsorbed alkoxy species. These species predominantly form on the Lewis acid sites of the alumina support. At least some of them are close enough to support Pt particles to block kink and edge sites at the interface from participating in the APR reaction. The reactivity of glucose is low when it is present in the cyclic hemi-acetal form, and unreactive surface species are formed when glucose adsorbs in the hemi-acetal form. The formation of strongly bound surface species, such as the cyclic hemi-acetals, is a plausible explanation for the low H_2 yield during APR of glucose. On the other hand, the formation of CO_B from glucose occurs more selectively than from sorbitol. This might be because it is easier to form the open-chain form of glucose on terrace sites, which are sufficiently far from the metal support interface. This open chain form contains the necessary aldehyde group to readily form CO by decarbonylation. In contrast, sorbitol needs to be dehydrogenated first, which may yield an aldehyde or a ketone. Ketones cannot be decarbonylated directly, and they could poison Pt sites, although no direct evidence for this was obtained in this study.

Since the water-gas shift reaction requires the activation of water in vicinity to the adsorbed CO, CO_B on terrace sites is more reactive for this reaction. Co-adsorbed feed molecules or their fragments can reduce the rate of the water-gas shift reaction by breaking up the required ensembles of Pt sites. At sufficiently high temperatures, inhibition by co-adsorbed species becomes less significant, and CO_L and CO_B can be converted into each other, which likely involves migration of the adsorbed CO to different sites.

Acknowledgments

Support from the Renewable Bioproducts Institute at the Georgia Institute of Technology in the form of a Paper Science and Engineering Fellowship for Jungeob So and financial support from the Nation Science Foundation (grant number: CBET-1705444) is gratefully acknowledged. The ^{13}C NMR measurement was performed using the Environmental Molecular Sciences Laboratory (Ringgold ID 130367), a DOE Office of Science User Facility sponsored by the Office of Biological and Environmental Research. Nancy Washton, Marcus Foston, and Blake Hammann are thanked for help with the NMR measurements.

Appendix A. Supplementary data

Supplementary material related to this article can be found, in the online version, at doi:https://doi.org/10.1016/j.mcat.2019.110423.

References

[1] G.W. Huber, S. Iborra, A. Corma, Synthesis of transportation fuels from biomass: chemistry, catalysts, and engineering, Chem. Rev. 106 (2006) 4044–4098.
[2] J.N. Chheda, G.W. Huber, J.A. Dumesic, Liquid-phase catalytic processing of biomass-derived oxygenated hydrocarbons to fuels and chemicals, Angew. Chem. Int. Ed. 46 (2007) 7164–7183.
[3] L.D. Schmidt, P.J. Dauenhauer, Chemical engineering: hybrid routes to biofuels, Nature 447 (2007) 914–915.
[4] J.W. Shabaker, R.R. Davda, G.W. Huber, R.D. Cortright, J.A. Dumesic, Aqueous-phase reforming of methanol and ethylene glycol over alumina-supported platinum catalysts, J. Catal. 215 (2003) 344–352.
[5] G.W. Huber, J.W. Shabaker, J.A. Dumesic, Raney Ni-Sn catalyst for H_2 production from biomass-derived hydrocarbons, Science 300 (2003) 2075–2077.
[6] R.R. Davda, J.W. Shabaker, G.W. Huber, R.D. Cortright, J.A. Dumesic, Aqueous-phase reforming of ethylene glycol on silica-supported metal catalysts, Appl. Catal. B-Environ. 43 (2003) 13–26.
[7] R.R. Davda, J.A. Dumesic, Renewable hydrogen by aqueous-phase reforming of glucose, Chem. Commun. (2004) 36–37.
[8] R.R. Davda, J.W. Shabaker, G.W. Huber, R.D. Cortright, J.A. Dumesic, A review of catalytic issues and process conditions for renewable hydrogen and alkanes by

aqueous-phase reforming of oxygenated hydrocarbons over supported metal catalysts, Appl. Catal. B-Environ. 56 (2005) 171–186.
[9] R.D. Cortright, R.R. Davda, J.A. Dumesic, Hydrogen from catalytic reforming of biomass-derived hydrocarbons in liquid water, Nature 418 (2002) 964–967.
[10] N. Li, G.W. Huber, Aqueous-phase hydrodeoxygenation of sorbitol with Pt/SiO_2–Al_2O_3: identification of reaction intermediates, J. Catal. 270 (2010) 48–59.
[11] A. Wawrzetz, B. Peng, A. Hrabar, A. Jentys, A.A. Lemonidou, J.A. Lercher, Towards understanding the bifunctional hydrodeoxygenation and aqueous phase reforming of glycerol, J. Catal. 269 (2010) 411–420.
[12] X.-K. Gu, B. Liu, J. Greeley, First-principles study of structure sensitivity of ethylene glycol conversion on platinum, ACS Catal. 5 (2015) 2623–2631.
[13] J.W. Shabaker, G.W. Huber, J.A. Dumesic, Aqueous-phase reforming of oxygenated hydrocarbons over Sn-modified Ni catalysts, J. Catal. 222 (2004) 180–191.
[14] G.W. Huber, R.D. Cortright, J.A. Dumesic, Renewable alkanes by aqueous-phase reforming of biomass-derived oxygenates, Angew. Chem. Int. Ed. 43 (2004) 1549–1551.
[15] J.W. Shabaker, G.W. Huber, R.R. Davda, R.D. Cortright, J.A. Dumesic, Aqueous-phase reforming of ethylene glycol over supported platinum catalysts, Catal. Lett. 88 (2003) 1–8.
[16] N. Luo, X. Fu, F. Cao, T. Xiao, P.P. Edwards, Glycerol aqueous phase reforming for hydrogen generation over Pt catalyst – effect of catalyst composition and reaction conditions, Fuel 87 (2008) 3483–3489.
[17] R. He, R.R. Davda, J.A. Dumesic, In situ ATR-IR spectroscopic and reaction kinetics studies of water-gas shift and methanol reforming on Pt/Al_2O_3 catalysts in vapor and liquid phases, J. Phys. Chem. B 109 (2005) 2810–2820.
[18] C.T. Campbell, G. Ertl, H. Kuipers, J. Segner, A molecular beam study of the catalytic oxidation of CO on a Pt(111) surface, J. Chem. Phys. 73 (1980) 5862–5873.
[19] C. Stampfl, M. Scheffler, Anomalous behavior of Ru for catalytic oxidation: a theoretical study of the catalytic reaction $CO + 1/2O_2 \rightarrow CO_2$, Phys. Rev. Lett. 78 (1997) 1500–1503.
[20] E.A. Wovchko, J.T. Yates, Activation of O_2 on a photochemically generated Rh^I site on an Al_2O_3 surface: low-temperature O_2 dissociation and CO oxidation, J. Am. Chem. Soc. 120 (1998) 10523–10527.
[21] J. Bergeld, B. Kasemo, D.V. Chakarov, CO oxidation on Pt(111) promoted by coadsorbed H_2O, Surf. Sci. 495 (2001) L815–L820.
[22] B.L. Hendriksen, J.W. Frenken, CO oxidation on Pt(110): scanning tunneling microscopy inside a high-pressure flow reactor, Phys. Rev. Lett. 89 (2002), 046101.
[23] A. Alavi, P. Hu, T. Deutsch, P.L. Silvestrelli, J. Hutter, CO oxidation on Pt(111): an ab initio density functional theory study, Phys. Rev. Lett. 80 (1998) 3650–3653.
[24] C. Akerlund, I. Zoric, B. Kasemo, A collision induced reaction: CO_2 production on O_2 and CO covered Pt(111), J. Chem. Phys. 104 (1996) 7359–7362.
[25] A.B. Mhadeshwar, D.G. Vlachos, Microkinetic modeling for water-promoted CO oxidation, water−gas shift, and preferential oxidation of CO on Pt, J. Phys. Chem. B 108 (2004) 15246–15258.
[26] X.-Q. Gong, P. Hu, R. Raval, The catalytic role of water in CO oxidation, J. Chem. Phys. 119 (2003) 6324–6334.
[27] C. Sievers, Y. Noda, Q. Long, E.M. Albuquerque, R.M. Rioux, S.L. Scott, Phenomena affecting catalytic reactions at solid-liquid interfaces, ACS Catal. 6 (2016) 8286–8307.
[28] S.D. Ebbesen, B.L. Mojet, L. Lefferts, The influence of water and pH on adsorption and oxidation of CO on Pd/Al_2O_3—an investigation by attenuated total reflection infrared spectroscopy, Phys. Chem. Chem. Phys. 11 (2009) 641–649.
[29] S.D. Ebbesen, B.L. Mojet, L. Lefferts, In situ ATR-IR study of CO adsorption and oxidation over Pt/Al_2O_3 in gas and aqueous phase: promotion effects by water and pH, J. Catal. 246 (2007) 66–73.
[30] J.R. Copeland, G.S. Foo, L.A. Harrison, C. Sievers, In situ ATR-IR study on aqueous phase reforming reactions of glycerol over a Pt/γ-Al_2O_3 catalyst, Catal. Today 205 (2013) 49–59.
[31] J. Rask, J. Kiss, Adsorption and surface reactions of acetaldehyde on alumina-supported noble metal catalysts, Catal. Lett. 101 (2005) 71–77.
[32] A.M. Silva, L.O.O. Costa, A.P.M.G. Barandas, L.E.P. Borges, L.V. Mattos, F.B. Noronha, Effect of the metal nature on the reaction mechanism of the partial oxidation of ethanol over CeO_2-supported Pt and Rh catalysts, Catal. Today 133–135 (2008) 755–761.
[33] M. El-Maazawi, A.N. Finken, A.B. Nair, V.H. Grassian, Adsorption and photocatalytic oxidation of acetone on TiO_2: an in situ transmission FT-IR study, J. Catal. 191 (2000) 138–146.
[34] K. Takanabe, K. Aika, K. Seshan, L. Lefferts, Sustainable hydrogen from bio-oil—steam reforming of acetic acid as a model oxygenate, J. Catal. 227 (2004) 101–108.
[35] A. Yee, S.J. Morrison, H. Idriss, A study of the reactions of ethanol on CeO_2 and Pd/CeO_2 by steady state reactions, temperature programmed desorption, and in situ FT-IR, J. Catal. 186 (1999) 279–295.
[36] J.R. Copeland, X.R. Shi, D.S. Sholl, C. Sievers, Surface interactions of C_2 and C_3 polyols with γ-Al_2O_3 and the role of coadsorbed water, Langmuir 29 (2013) 581–593.
[37] J.R. Copeland, I.A. Santillan, S.M. Schimming, J.L. Ewbank, C. Sievers, Surface interactions of glycerol with acidic and basic metal oxides, J. Phys. Chem. C 117 (2013) 21413–21425.
[38] B.N. Zope, R.J. Davis, Inhibition of gold and platinum catalysts by reactive intermediates produced in the selective oxidation of alcohols in liquid water, Green Chem. 13 (2011) 3484.
[39] S. Brunauer, P.H. Emmett, E. Teller, Adsorption of gases in multimolecular layers, J. Am. Chem. Soc. 60 (1938) 309–319.
[40] E.P. Barrett, L.G. Joyner, P.P. Halenda, The determination of pore volume and area distributions in porous substances. I. Computations from nitrogen isotherms, J. Am. Chem. Soc. 73 (1951) 373–380.
[41] J. Datka, A.M. Turek, J.M. Jehng, I.E. Wachs, Acidic properties of supported niobium oxide catalysts—an infrared-spectroscopy investigation, J. Catal. 135 (1992) 186–199.
[42] K. Wefers, C. Misra, Oxides and Hydroxides of Aluminum, 2nd ed., Alcoa Research Laboratories, 198792.
[43] A.F. Holleman, E. Wiberg, Inorganic Chemistry, 34th ed., Academic Press, Berlin, 20011884.
[44] M.I. Zaki, M.A. Hasan, F.A. Al-Sagheer, L. Pasupulety, In situ FTIR spectra of pyridine adsorbed on SiO_2–Al_2O_3, TiO_2, ZrO_2 and CeO_2: general considerations for the identification of acid sites on surfaces of finely divided metal oxides, Colloid Surf. A-Physicochem. Eng. Asp. 190 (2001) 261–274.
[45] A. Bourane, O. Dulaurent, D. Bianchi, Heats of adsorption of linear and multibound adsorbed CO species on a Pt/Al_2O_3 catalyst using in situ infrared spectroscopy under adsorption equilibrium, J. Catal. 196 (2000) 115–125.
[46] N.B. Colthup, L.H. Daly, S.E. Wiberley, Introduction to Infrared and Raman Spectroscopy, Academic Press, 1990547.
[47] J.R. McManus, M. Salciccioli, W. Yu, D.G. Vlachos, J.G. Chen, J.M. Vohs, Correlating the surface chemistry of C_2 and C_3 aldoses with a C6 sugar: reaction of glucose, glyceraldehyde, and glycolaldehyde on Pd(111), J. Phys. Chem. C 116 (2012) 18891–18898.
[48] D.J.M. de Vlieger, B.L. Mojet, L. Lefferts, K. Seshan, Aqueous phase reforming of ethylene glycol – role of intermediates in catalyst performance, J. Catal. 292 (2012) 239–245.
[49] D. Ferri, T. Bürgi, A. Baiker, Pt and Pt/Al_2O_3 thin films for investigation of catalytic solid−liquid interfaces by ATR-IR spectroscopy: CO adsorption, H_2 induced reconstruction and surface-enhanced absorption, J. Phys. Chem. B 105 (2001) 3187–3195.
[50] A.C. Garcia, M.J. Kolb, C. van Nierop y Sanchez, J. Vos, Y.Y. Birdja, Y. Kwon, G. Tremiliosi-Filho, M.T.M. Koper, Strong impact of platinum surface structure on primary and secondary alcohol oxidation during electro-oxidation of glycerol, ACS Catal. 6 (2016) 4491–4500.
[51] A. Bourane, S. Derrouiche, D. Bianchi, Impact of Pt dispersion on the elementary steps of CO oxidation by O_2 over Pt/Al_2O_3 catalysts, J. Catal. 228 (2004) 288–297.
[52] H. Hanawa, K. Kunimatsu, H. Uchida, M. Watanabe, In situ ATR-FTIR study of bulk CO oxidation on a polycrystalline Pt electrode, Electrochim. Acta 54 (2009) 6276–6285.
[53] D.S. Paz, S. Damyanova, L.R. Borges, J.B.O. Santos, J.M.C. Bueno, Identifying the adsorbed active intermediates on Pt surface and promotion of activity through the redox CeO_2 in preferential oxidation of CO in H_2, Appl. Catal. A-Gen. 548 (2017) 164–178.
[54] A.D. Allian, K. Takanabe, K.L. Fujdala, X. Hao, T.J. Truex, J. Cai, C. Buda, M. Neurock, E. Iglesia, Chemisorption of CO and mechanism of CO oxidation on supported platinum nanoclusters, J. Am. Chem. Soc. 133 (2011) 4498–4517.
[55] E.V. Benvenutti, L. Franken, C.C. Moro, C.U. Davanzo, FTIR study of hydrogen and carbon monoxide adsorption on Pt/TiO_2, Pt/ZrO_2, and Pt/Al_2O_3, Langmuir 15 (1999) 8140–8146.
[56] C.S. Kim, C. Korzeniewski, W.J. Tornquist, Site specific co-adsorption at Pt(335) as probed by infrared spectroscopy: structural alterations in the CO adlayer under aqueous electrochemical conditions, J. Chem. Phys. 100 (1994) 628–630.
[57] N. Kizhakevariam, X. Jiang, M.J. Weaver, Infrared spectroscopy of model electrochemical interfaces in ultrahigh vacuum: the archetypical case of carbon monoxide/water coadsorption on Pt(111), J. Chem. Phys. 100 (1994) 6750–6764.
[58] S.C. Chang, M.J. Weaver, In situ infrared spectroscopy at single-crystal metal electrodes: an emerging link between electrochemical and ultrahigh-vacuum surface science, J. Phys. Chem. 95 (1991) 5391–5400.
[59] W. van Bronswijk, H.R. Watling, Z. Yu, A study of the adsorption of acyclic polyols on hydrated alumina, Colloid Surf. A-Physicochem. Eng. Asp. 157 (1999) 85–94.
[60] R.M. Ravenelle, J.R. Copeland, A.H. Van Pelt, J.C. Crittenden, C. Sievers, Stability of Pt/γ-Al_2O_3 catalysts in model biomass solutions, Top. Catal. 55 (2012) 162–174.
[61] S. Proch, J. Herrmannsdorfer, R. Kempe, C. Kern, A. Jess, L. Seyfarth, J. Senker, Pt@MOF-177: synthesis, room-temperature hydrogen storage and oxidation catalysis, Chem.-Eur. J. 14 (2008) 8204–8212.
[62] R.M. Ravenelle, J.R. Copeland, W.-G. Kim, J.C. Crittenden, C. Sievers, Structural changes of γ-Al_2O_3-supported catalysts in hot liquid water, ACS Catal. 1 (2011) 552–561.
[63] S.G. Li, V.A. Tuan, J.L. Falconer, R.D. Noble, Separation of 1,3-propanediol from glycerol and glucose using a ZSM-5 zeolite membrane, J. Membr. Sci. 191 (2001) 53–59.
[64] C. Keresszegi, D. Ferri, T. Mallat, A. Baiker, Unraveling the surface reactions during liquid-phase oxidation of benzyl alcohol on Pd/Al2O3: an in situ ATR-IR study, J. Phys. Chem. B 109 (2005) 958–967.
[65] V.A. Yaylayan, A.A. Ismail, S. Mandeville, Quantitative determination of the effect of pH and temperature on the keto form of d-fructose by FT IR spectroscopy, Carbohydr. Res. 248 (1993) 355–360.
[66] G.W. Huber, J.W. Shabaker, S.T. Evans, J.A. Dumesic, Aqueous-phase reforming of ethylene glycol over supported Pt and Pd bimetallic catalysts, Appl. Catal. B-Environ. 62 (2006) 226–235.